Toward Structurally Defined Carbon Dots as Ultracompact Fluorescent Probes

Gregory Ethan LeCroy,[†] Sumit Kumar Sonkar,[†] Fan Yang,[†] L. Monica Veca,[‡,*] Ping Wang,[†] Kenneth N. Tackett, II,[†] Jing-Jiang Yu,[§] Eugeniu Vasile,[⊥] Haijun Qian,[†] Yamin Liu,[†] Pengju (George) Luo,[†] and Ya-Ping Sun[†,*]

[†]Department of Chemistry and Laboratory for Emerging Materials and Technology, Clemson University, Clemson, South Carolina 29634, United States, [‡]National Institute for Research and Development in Microtechnologies, IMT-Bucharest, Bucharest 077190, Romania, [§]Nanotechnology Measurements Division, Agilent Technologies, Inc., Chandler, Arizona 85226, United States, and [⊥]Department of Oxide Materials and Nanomaterials, Faculty of Applied Chemistry and Material Science, University Politehnica of Bucharest, Bucharest, Romania

ABSTRACT There has been much discussion on the need to develop fluorescent quantum dots (QDs) as ultracompact probes, with overall size profiles comparable to those of the genetically encoded fluorescent tags. In the use of conventional semiconductor QDs for such a purpose, the beautifully displayed dependence of fluorescence color on the particle diameter becomes a limitation. More recently, carbon dots have emerged as a new platform of QD-like fluorescent nanomaterials. The optical absorption and fluorescence emissions in carbon dots are not bandgap in origin, different from those in conventional semiconductor QDs. The absence of any theoretically defined fluorescence color - dot size relationships in carbon dots may actually be exploited as a unique advantage in the size reduction toward having carbon dots serve as ultracompact QD-like fluorescence probes. Here we report on carbon dots of less than 5 nm in the overall dot diameter with the use of 2,2′-(ethylenedioxy)bis(ethylamine) (EDA) molecules for the carbon particle surface passivation. The EDA-carbon dots were found to be brightly fluorescent, especially over the spectral range of green fluorescent protein. These aqueous soluble smaller carbon dots also enabled more quantitative characterizations, including the use of solution-phase NMR techniques, and the results suggested that the dot structures were relatively simple and better-defined. The potential for these smaller carbon dots to serve as fluorescence probes of overall sizes comparable to those of fluorescent proteins is discussed.

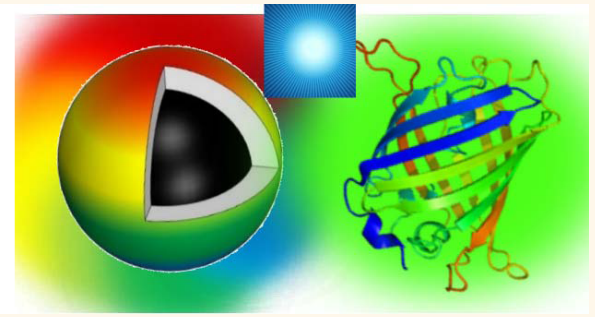

KEYWORDS: carbon dots · fluorescence · green fluorescence protein (GFP) · quantum dots · bioimaging · molecular probes · ultracompact probes · functionalized nanoparticles

Fluorescent semiconductor nanocrystals, generally referred to as quantum dots (QDs) for the quantum confinement effect in these nanomaterials, have attracted much attention for their serving as optical probes in biomedical and other applications.[1,2] Among the most popular QDs, some of which are now commercially available, are those based on cadmium salts, especially CdSe/ZnS core−shell nanostructures with various surface coatings for organic or aqueous compatibilities.[3−5] Strong cases have been made in the literature on using QDs to replace organic dyes and in some applications genetically encoded fluorescent tags.[1,2,6] Among many widely considered advantageous properties of conventional semiconductor QDs, a unique feature due to the quantum confinement effect is the beautiful display of different fluorescence colors for QDs of different sizes. However, the defined color−size dependence also limits any dot size variation for a specific fluorescence color. For the more established CdSe/ZnS QDs with the necessary surface coating (for solubility and/or compatibility needs) as fluorescence probes, the probe size profiles are typically on the order of 10 nm in diameter.[6−8] Therefore, there has been increasing interest in a reduction of the probe size, targeting similar size profiles to those of many commonly used fluorescent proteins (green fluorescent protein, or GFP, for example),[9] for which strategies such as the use of a thinner coating on the QD surface have been pursued.[1,10−12]

In terms of application potential, ultracompact probes (referring to structurally compact and very small in the overall probe size) offer additional and sometimes unique

* Address correspondence to monica.veca@imt.ro, syaping@clemson.edu.

Received for review December 27, 2013 and accepted April 6, 2014.

Published online April 07, 2014
10.1021/nn406628s

opportunities, with specific biologically relevant examples including their less interference with or perturbation to the biological events in the cells being probed[13−15] and more favorable renal clearance, for which a threshold probe size around 5.5 nm was determined.[16] There were also studies in which issues with the use of larger nanoparticles were identified, such as their accumulation in leaky vasculature or in solid tumors, thus potentially inhibiting clearance and increasing the likelihood of long-term toxicity effect.[17−19] Most of the recently pursued ultracompact probes were based on metal or metal oxide nanoparticles, especially sub-5 nm gold nanoparticles[20,21] and gadolinium or iron oxide nanoparticles for MRI tracking applications.[22,23] As a demonstration on the critical effect of probe size, gold nanoparticles of 2.4 nm in diameter were found in the cell nucleus, 5.5−8.2 nm in the cytoplasm, and 16 nm or larger mostly outside the cell.[21]

Carbon dots have emerged as a new platform of QD-like fluorescent nanomaterials,[24] with competitive optical performance under one- and multiphoton excitation conditions and their being generally nontoxic in nature.[25−39] Presently more fluorescent carbon dots are those of small carbon nanoparticles with the particle surface passivated by chemical functionalization with oligomeric or polymeric species. For example, with the oligomeric poly(ethylene glycol) diamine (PEG_{1500N}) as surface passivation agent, the PEG_{1500N}-carbon dots exhibited fluorescence quantum yields of more than 50%.[34] Mechanistically, both the optical absorption and fluorescence emissions in carbon dots are not band gap in origin, due instead to π-plasmon and radiative recombination of the surface-confined electrons and holes, respectively,[39,40] different from those in conventional semiconductor QDs. The absence of any theoretically defined fluorescence color−dot size relationships in carbon dots may actually be exploited as a unique advantage in the size reduction toward having carbon dots serve as ultracompact QD-like fluorescence probes. More specifically, there has been extensive recent discussion on the push to reduce the sizes of fluorescence probes (mostly those based on conventional semiconductor QDs with the necessary surface coating) to less than 5 nm in diameter.[9] In this regard, the PEG_{1500N}-carbon dots referred to above had an average core carbon nanoparticle size of about 3 nm,[34] but the overall dot profiles were on average significantly larger due to the use of the relatively large PEG_{1500N} molecules (average molecular weight ~1500) for carbon particle surface passivation *via* chemical functionalization. The expectation was such that a reduction in the size of the surface functionalization molecules would not only add less to the overall profile (the core carbon nanoparticle + surface passivation layer) of each carbon dot but also be more selective toward the solubilization of smaller carbon nanoparticles in the dot synthesis, resulting in smaller carbon dots and their corresponding fluorescence probes.

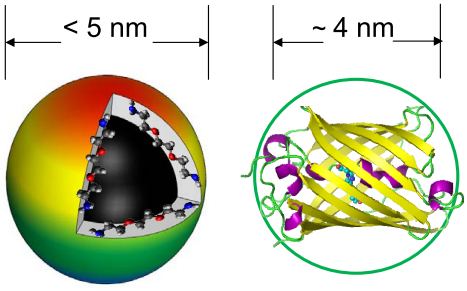

Figure 1. Cartoon illustration (left) of an EDA-carbon dot, which is essentially a special "core−shell" nanostructure with a small carbon nanoparticle as the core and a soft shell of tethered EDA molecules, and (right) green fluorescent protein with the size profile highlighted.

Here we report on carbon dots of less than 5 nm in overall dot diameter with the use of 2,2′-(ethylenedioxy)-bis(ethylamine) (EDA, $H_2NCH_2CH_2OCH_2CH_2OCH_2CH_2NH_2$) molecules for carbon particle surface functionalization−passivation (Figure 1). The EDA-carbon dots were found to be brightly fluorescent, especially over the GFP spectral range. These aqueous soluble smaller carbon dots also enabled more quantitative characterizations, including the use of solution-phase NMR techniques, and the results suggested that the dot structures were relatively simple and better defined. The potential for these smaller carbon dots to serve as fluorescence probes of overall sizes comparable to those of fluorescent proteins (Figure 1)[41−43] is also discussed.

RESULTS AND DISCUSSION

Precursor carbon nanoparticles were obtained from the commercially supplied sample of carbon nanopowders in a procedure that included refluxing the as-supplied sample in an aqueous nitric acid solution, dialysis, centrifuging to retain the supernatant (with a higher population of smaller particles), and then the removal of water.[34] The nanoparticles were functionalized with EDA molecules under amidation reaction conditions. Briefly, the sample of carbon nanoparticles was first refluxed in neat thionyl chloride and then mixed well with carefully dried EDA (liquid at ambient temperature). The mixture was heated to 120 °C and vigorously stirred for the reaction under nitrogen protection. The reaction mixture was dispersed in water for centrifugation to retain the supernatant, followed by purification through a gel column (packed in-house by using commercially supplied Sephadex G-100 gel)[44] to isolate the targeted carbon dots (EDA-functionalized carbon nanoparticles, Figure 1) of bright fluorescence emissions. The carbon dots sample was further purified in dialysis against fresh water to remove residual small molecular species including free EDA molecules, yielding a clean aqueous solution of the purified carbon dots (designated as

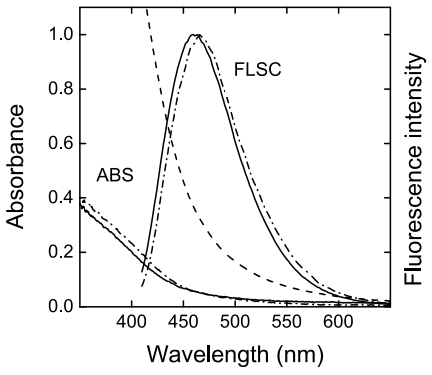

Figure 2. Absorption (ABS) and fluorescence (FLSC, 400 nm excitation) spectra of the EDA-carbon dots (— and - - - for ABS of a concentrated solution) and the ^{13}C-enriched EDA-carbon dots (- · - · -).

EDA-carbon dots). According to results from the quantitative optical absorption measurement of the EDA-carbon dots (Figure 2), in which the amount of core carbon nanoparticles was calculated with the separately determined molar absorptivity values[45] and the amount was compared to that of the precursor carbon nanoparticles, the estimated overall reaction yield was around 10% (the percentage of the precursor carbon nanoparticles converted to the core carbon nanoparticles in the final purified EDA-carbon dots).

The EDA-carbon dots were characterized by using atomic force microscopy (AFM) for the determination of overall dot sizes. The AFM specimen was prepared by dropping an aqueous solution of a selected dot concentration onto the mica surface, followed by the evaporation of water. Shown in Figure 3 are representative AFM imaging results for the EDA-carbon dots, in which according to height analyses an overwhelming majority of the dots were less than 5 nm in diameter. Multiple AFM images were used in the same height analyses to produce a data set for about 280 dots, and as also shown in Figure 3, the statistical analysis with a simple Gaussian function yielded an average dot size of 4.1 nm. The results are consistent with the expectation that the EDA-carbon dots should be smaller than the PEG_{1500N}-carbon dots, which averaged around 5 nm in diameter according to previous investigations.[34,39] The conclusion is also supported by the results from transmission electron microscopy (TEM) imaging experiments.

For the PEG_{1500N}-carbon dots reported previously, the TEM imaging enabled the size characterization of the core carbon nanoparticles, averaging 3 nm in diameter,[34] as the organic surface functionalization molecules (PEG_{1500N}) were largely transparent in contrast with the carbon core. For some dots in which the core carbon nanoparticles were more crystalline, the size measurements could also benefit from the more defined lattice fringes (Figure 3). However, in order to apply the TEM imaging to the determination of overall size profiles that include the surface passivation layer in carbon dots (Figure 1), the approach of doping the dots

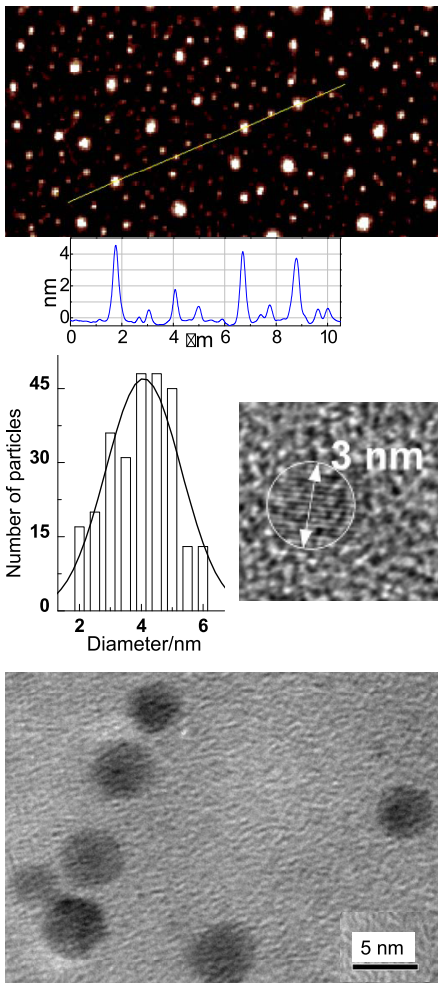

Figure 3. (Top) AFM imaging results for the EDA-carbon dots on mica substrate, with height profiles of some dots along the line highlighted. (Middle) (left) Size distribution based on height analyses of multiple AFM images, fitted with the Gaussian distribution curve, and (right) a high-resolution TEM image illustrating the carbon core in a carbon dot.[34] (Bottom) TEM image of the gold-doped EDA-carbon dots.

with materials of high electron density has found some success.[46] In this work the EDA-carbon dots were doped with gold metal in a simple photolysis procedure, with visible-light photoirradiation of the dots in an aqueous solution of the Au(III) compound $HAuCl_4$.[46] The gold-doped dots were readily detected in TEM imaging for the improved dispersion into individual dots on the TEM grid, in addition to the increased electron densities. The TEM images (Figure 3) thus obtained were consistent with the AFM results (Figure 3), which suggested that the EDA-carbon dots should be mostly less than 5 nm in diameter for the overall dot profiles including the surface passivation layer of tethered EDA molecules.

The optical transitions in carbon dots are due to the π-plasmon absorption of the core carbon nanoparticles, namely, the "chromophores" in the dots.[45] The absorption (Figure 2) is relatively strong, with

the observed per-carbon molar absorptivities of 50−100 $M_{C\ atom}^{-1}$ cm^{-1} in the 400−450 nm region, where $M_{C\ atom}$ denotes molar concentration in terms of carbon atoms in the core carbon nanoparticles (assuming no other elements) for the carbon dots in a solution. For a carbon core size of 3 nm in diameter, the number of carbon atoms in the core was estimated to be around 1700, thus per-dot molar absorptivities of approximately 85 000−170 000 $M_{C\text{-particle}}^{-1}$ cm^{-1} for the same wavelength region, where $M_{C\text{-particle}}$ refers to the molar concentration of the carbon dots with 3 nm diameter carbon cores. The per-dot molar absorptivities should obviously be sensitive to the dot diameter. For example, the EDA-carbon dots with a carbon core of 3.5 nm in diameter would have absorptivities up to approximately 250 000 $M_{C\text{-particle}}^{-1}$ cm^{-1}. These estimates accounted for only carbons in the nanoparticle cores (again the visible chromophores) in the carbon dots, with the carbons in EDA molecules excluded for their being nonabsorptive in the visible spectral region.

The fluorescence spectrum of the EDA-carbon dots in aqueous solution, with excitation at 400 nm, is also shown in Figure 2. It is relatively broad, similar to those of carbon dots with other surface-functionalization molecules. The green fluorescence emissions are associated with quantum yields around 30%, determined in reference to 9,10-bis(phenylethynyl)anthracene as a standard (quantum yield of unity, calibrated against the quinine sulfate standard).[47,48] The fluorescence properties of the EDA-carbon dots were apparently stable with respect to further sample purification effort on removing any loosely attached EDA molecules from the carbon dots in vigorous dialysis. Both the fluorescence spectrum and quantum yield remained the same after the repeated dialysis procedures, suggesting that the aqueous dispersed EDA-carbon dots were structurally robust, with the EDA functionalization on the dot surface being either covalent or associated with bonding-like strong interactions. More generally, the EDA-carbon dots are similar to the more extensively studied PEG_{1500N}-carbon dots in terms of excellent chemical and photochemical stabilities.

In molecular imaging and related uses, the performance of fluorescence probes is often measured in terms of the relative brightness, expressed as (molar absorptivity) × (fluorescence quantum yield). For the EDA-carbon dots of the carbon core at 3 nm in diameter, the corresponding fluorescence probes of less than 5 nm in diameter and with green fluorescence emissions could have a relative brightness as high as 50 000. As a rough comparison, the relative brightness values quoted in the literature on the commonly used GFP and derivatives are on the order of 30 000.[49]

Structurally an EDA-carbon dot is simply a small carbon nanoparticle with a thin layer of tethered EDA molecules on the particle surface (Figure 1). The

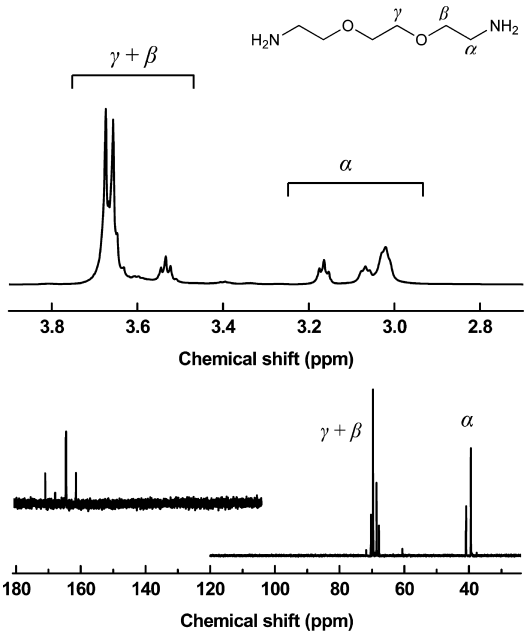

Figure 4. (Top) ^{1}H NMR spectrum of the EDA-carbon dots. (Bottom) ^{13}C NMR spectrum of the EDA-carbon dots and (inset on the left) the lower-field portion of the spectrum for the ^{13}C-enriched EDA-carbon dots.

aqueous dispersion of EDA-carbon dots is solution-equivalent in appearance and in properties, suitable for solution-phase NMR characterizations. The ^{1}H NMR spectrum of the EDA-carbon dots (Figure 4), due to the tethered EDA molecules on the dot surface, shows broader signals than those in the spectrum of free EDA, consistent with the reduced mobility of the EDA molecules attached to carbon nanoparticles. Also consistent with the attachment is the lower symmetry for the particle-bound EDA species, with ^{1}H NMR signals for the three sets of protons in free EDA (Figure 4, γ: singlet, β: triplet, and α: triplet) split into multiple peaks in two groups, one for γ and β protons and the other for α protons (Figure 4). The relative integrations between $\gamma+\beta$ and α proton signals are about 2.3 to 1, larger than the theoretical ratio of 2 to 1. A question was then on the assignment of the signal around 3.5 ppm, namely, the possibility for its being due to α protons. Such a possibility could be eliminated on the basis of correlation spectroscopy (COSY) results, which clearly identified the coupling of the broad 3.5 ppm signal with those of the α protons. Therefore, an alternative explanation is such that the NMR signal integration for the α protons is distorted by these protons being closer to the core carbon nanoparticles in the carbon dots. The ^{13}C NMR spectrum of the EDA-carbon dots (Figure 4) shows similarly two groups of peaks, again one for γ and β carbons and the other for α carbons, but no meaningful peaks that could be assigned to the core carbon nanoparticles. Results from the FT-IR characterization were generally consistent with the NMR results. The carbon nanoparticles

before the EDA functionalization exhibited only weak absorptions in the 1550−1750 cm^{-1} region, suggesting the presence but low population of oxygen-containing moieties (such as carboxylic acids). These absorption features could still be identified in the spectrum of the EDA-carbon dots, although only to a rather limited extent due to their overlapping with the more substantial absorption of EDA over the same spectral region (1400−1700 cm^{-1}).[50,51] Overall the FT-IR spectrum of the EDA-carbon dots is similar to that of EDA molecules in terms of major spectral features, but with some peak broadening probably due to the association of EDA with carbon nanoparticles in the carbon dots. Therefore, the FT-IR results were not as useful as desired in the elucidation of structural details, but overall did seem to suggest that there were no significant changes to the EDA chemical structure, such as those that might create visible chromophores, as a result of the functionalization chemistry (probably as expected for the rather mild reaction conditions).

Further ^{13}C NMR characterization was on the similarly prepared EDA-carbon dots with the core carbon nanoparticles ^{13}C-enriched. Experimentally, the carbon soot sample containing ^{13}C-enriched carbon nanoparticles was produced in the arc-discharge of two graphite rods, one of which was made hollow and then filled with a mixture of commercially supplied ^{13}C powders and graphite cement.[31] According to quantitative Raman spectral shift measurements, the precursor carbon nanoparticles for the functionalization with EDA molecules had a ^{13}C content of 10−15%, and the same ^{13}C enrichment in the resulting carbon dots should be expected. As compared in Figure 2, the absorption and fluorescence spectra of the ^{13}C-enriched EDA-carbon dots are rather similar to those without the ^{13}C enrichment. For the ^{13}C NMR results of the ^{13}C-enriched EDA-carbon dots, there are no additional peaks in the aliphatic region nor any detectable aromatic signals (Figure 4). The relatively weak but meaningful peaks in the 175−160 ppm region (Figure 4) may be assigned to carbonyl carbons on the core carbon nanoparticles. However, since smaller carbon nanoparticles are expected to have more diverse surface defects or carbon sites, the ^{13}C NMR signals of the EDA-carbon dots, whose carbon cores are definitely at the smaller side, are subject to more significant broadening effects. Therefore, the observed carbonyl signals likely represent only some in the minority that could be detected. The results are informative in the sense that they are consistent with the expected diverse carbon environment on the core carbon nanoparticle surface.

It is interesting that the functionalization results for the precursor carbon nanoparticles without and with the ^{13}C-enrichment were rather similar, as the nanoparticles were from different production methods,

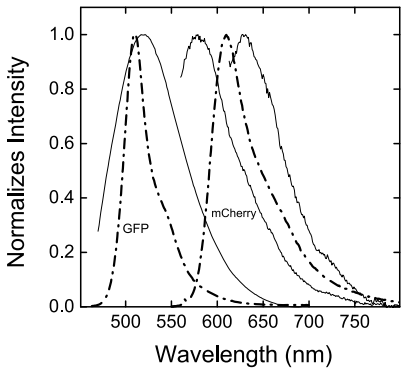

Figure 5. Fluorescence spectra of the EDA-carbon dots excited at (from left to right, −) 440 nm (fluorescence quantum yield $\Phi_F \approx 30\%$), 550 nm ($\Phi_F \approx 7\%$), and 600 nm ($\Phi_F \approx 3.7\%$), with spectra of the fluorescent proteins GFP and mCherry also shown for comparison.

laser processing for the commercially supplied sample *vs* arc-discharge for the ^{13}C-enriched sample. The former is generally somewhat more crystalline than the latter. Therefore, the nearly identical optical properties of their resulting EDA-carbon dots suggest stability with the synthesis method for more consistent production of the carbon dots from different sources of precursor carbon nanoparticles.

The EDA-carbon dots as ultracompact fluorescence probes, with overall size profiles of less than 5 nm in diameter, are not limited to green fluorescence only, with emissions also observed in other colors at different excitation wavelengths (Figure 5). Again for a rough comparison, the fluorescent protein mCherry, whose spectrum is also included in the figure, has a similar size profile of around 4 nm.[52] Previous results suggested that the same carbon dots could be used for fluorescence imaging at different colors, though not with the same sensitivities.[39] Further investigations targeting color variations of bright fluorescence emissions over the visible spectrum, such as the exploration of other carbon nanoparticle surface passivation schemes, while maintaining the overall size profiles of the carbon dots are warranted, thus to take full advantage of their different fluorescence emission mechanism from that in conventional semiconductor QDs.

The development of ultracompact fluorescence probes based on carbon dots offers significant values both fundamentally and technologically. On the fundamental side, the experimental confirmation on the preparation of the very small carbon dots of multiple fluorescence colors in the visible spectrum serves to support the existing mechanistic framework for carbon dots, namely, that the fluorescence emissions are due to the radiative recombination of the trapped or confined electrons and holes from the initial charge separation following the photoexcitation. The emission colors may be affected by changes in the core carbon nanoparticle size, with associated changes in the particle surface properties such as the surface curvature,

trapping sites, different passivation effects, *etc*., but not limited by any defined relationships as in conventional semiconductor QDs. Therefore, it seems reasonable to argue that the reduction of carbon dot size profile in this work may represent just the beginning, with more room for further miniaturization through the production or harvesting from mixtures of even smaller carbon nanoparticles for surface passivation by a thinner layer of organic materials. Technologically, the fluorescence probes of size profiles comparable to or eventually smaller than those of the genetically encoded fluorescent tags may open up many new application opportunities, which should also benefit from the other known properties of carbon dots, such as physicochemical and photochemical stabilities, nonblinking, and the intrinsically available organic functional groups on the probe surface amenable to bioconjugations and other purposes.

One of the applications targeted in the literature for small fluorescence probes is in cell imaging.[1,9] Previous investigations demonstrated that carbon dots with the surface passivation molecules containing abundant amino moieties were readily taken up by cells, enabling fluorescence imaging of the cells by using confocal or multiphoton fluorescence microscopy techniques.[39] Similar cellular uptake of the EDA-carbon dots may be expected, and evaluations related to their potential uses in fluorescence cell imaging will be pursued.

CONCLUSION

The reported work demonstrated that small PEG diamine molecules could be used to functionalize carbon nanoparticles to produce surface-passivated carbon dots with optical properties similar to those of the more extensively studied PEG_{1500N}-carbon dots. The results suggest generally excellent solubility characteristics of carbon dots, as the passivation agent layer in the overall structure of the EDA-carbon dots is relatively small. Smaller functionalization molecules are expected to be in favor of smaller carbon nanoparticles in the solubilization, resulting in more compact carbon dots. In fact, the EDA-carbon dots were found to be comparable in size to GFPs, with expanded application potential in bioimaging and beyond. The demonstration on the reduction in probe size without sacrificing the intrinsic properties of carbon dots may stimulate further investigations on the preparation of bright fluorescent probes of even smaller footprints.

EXPERIMENTAL SECTION

Materials. Carbon nanopowder (<50 nm, purity 99+%), ^{13}C powders (isotopic purity 99%), and 2,2′-(ethylenedioxy)bis-(ethylamine) were purchased from Sigma-Aldrich, and fine-extruded graphite rods (carbon content 99+%) from Graphitestore, Inc. Thionyl chloride (>99%) was obtained from Alfa Aesar, nitric acid from VWR, and Sephadex G-100 gel from GE Healthcare. Dialysis membrane tubing (cutoff molecular weight 500) was supplied by Spectrum Laboratories. Water was deionized and purified by being passed through a Labconco WaterPros water purification system.

Measurements. Optical absorption spectra were recorded on a Shimadzu UV2501-PC spectrophotometer. Fluorescence spectra were measured on a Jobin-Yvon emission spectrometer equipped with a 450 W xenon source, Gemini-180 excitation and Tirax-550 emission monochromators, and a photon-counting detector (Hamamatsu R928P PMT at 950 V). The nonlinear instrumental responses at both excitation and emission sides of the spectrometer were corrected by using separately determined correction factors with respect to different excitation and emission wavelengths.[48] Raman spectra were obtained on a Jobin-Yvon T64000 Raman spectrometer equipped with a Melles-Griot He−Ne laser (35 mW) for 632.8 nm excitation, a triple monochromator, a liquid-nitrogen-cooled symphony detector, and an Olympus BX-41 microscopy for sampling. FT-IR spectra were collected on a Thermo-Nicolet Nexus 670 FT-IR/NIR spectrometer, with the samples for analysis deposited on the surface of a KBr crystal pellet. NMR measurements were performed on a Bruker Avance 500 NMR spectrometer. Atomic force microscopy images were acquired in the acoustic ac mode on a Molecular Imaging PicoPlus AFM system equipped with a multipurpose scanner and a Nano-World point probe NCH sensor. The height profile analysis was assisted by using the SjPIP software distributed by Image Metrology. Transmission electron microscopy images were obtained on a Hitachi H9500 TEM system.

^{13}C-Enriched Carbon Nanoparticles. The carbon soot containing the nanoparticles was obtained in the arc-discharge production, as reported previously.[31] A graphite rod was made hollow and then filled with a mixture of the commercially supplied ^{13}C powders and graphite cement. The discharge chamber was purged with helium and then stabilized to 1 atm (101.325 kPa) in a helium atmosphere. The rods were vaporized with a direct current of 70 A (28 V). The as-produced carbon soot was collected and dispersed in dimethylformamide (DMF) with ultrasonication (Crest Ultrasonics, model 950 DA, 50−60 Hz) for 24 h. The DMF was removed by evaporation, and the carbon particles were recovered. The ^{13}C content in the sample was estimated in terms of Raman spectral shifts, as validated previously.[31]

EDA-Carbon Dots. The precursor carbon nanoparticles were refluxed in an aqueous nitric acid solution (2.6 M) for 12 h, dialyzed against fresh water, and then centrifuged at 1000*g* to retain the supernatant. The recovered sample was refluxed in neat thionyl chloride for 12 h. Upon the removal of excess thionyl chloride, the sample (50 mg) was mixed well with carefully dried EDA liquid (600 mg) in a round-bottom flask, heated to 120 °C, and vigorously stirred under nitrogen protection for 3 days. The reaction mixture back at room temperature was dispersed in water and then centrifuged at 20800*g* to retain the supernatant. The solution was filtrated through a Sephadex G-100 column (packed in house with commercially supplied gel sample),[39,44] and the colored section with high fluorescence quantum yields was collected, followed by dialysis against fresh water (dialysis tubing cutoff molecular weight 500) to yield an aqueous solution of the EDA-carbon dots. ^{1}H NMR (500 MHz, D_2O) δ 3.67 (m, br), 3.54 (m, br), 3.17 (m, br), 3.07 (m, br), 3.03 (m, br) ppm; ^{13}C NMR (125 MHz, D_2O) δ 164.76, 71.78, 70.33, 69.69, 67.85, 40.93, 39.45 ppm.

The ^{13}C-enriched EDA-carbon dots were prepared from the ^{13}C-enriched precursor carbon nanoparticles by following the same experimental procedures. ^{1}H NMR (500 MHz, D_2O) δ 3.65 (m, br), 3.53 (m, br), 3.17 (m, br), 2.98 (m, br), 2.91 (m, br) ppm; ^{13}C NMR (125 MHz, D_2O) δ 171.12, 164.81, 164.63, 161.56, 71.75, 70.34, 69.65, 69.61, 68.81, 40.98, 39.64 ppm.

For the gold metal doping of the EDA-carbon dots (for TEM imaging), an aqueous dispersion of the EDA-carbon dots was mixed with an aqueous solution of the Au(III) compound $HAuCl_4$, and the mixture was irradiated with visible light.[46]

The doping level was kept relatively low, as monitored in terms of the gold plasmon absorption band.

Conflict of Interest: The authors declare no competing financial interest.

Acknowledgment. Financial support from NSF (Y.-P.S.), the Romanian National Authority for Scientific Research (CNCS-UEFISCDI, project PNII-ID-PCCE-2011-2-0069) (L.M.V.), and the South Carolina Space Grant Consortium (Y.-P.S.) is gratefully acknowledged.

REFERENCES AND NOTES

1. Kairdolf, B. A.; Smith, A. M.; Stokes, T. H.; Wang, M. D.; Young, A. N.; Nie, S. Semiconductor Quantum Dots for Bioimaging and Biodiagnostic Applications. *Annu. Rev. Anal. Chem.* **2013**, *6*, 143.
2. Freeman, R.; Willner, I. Optical Molecular Sensing with Semiconductor Quantum Dots (QDs). *Chem. Soc. Rev.* **2012**, *41*, 4067–4085.
3. Hines, M. A.; Philippe, G.-S. Synthesis and Characterization of Strongly Luminescing ZnS-Capped CdSe Nanocrystals. *J. Phys. Chem.* **1996**, *100*, 468–471.
4. Uyeda, H. T.; Medintz, I. L.; Jaiswal, J. K.; Simon, S. M.; Mattoussi, H. Synthesis of Compact Multidentate Ligands to Prepare Stable Hydorphilic Quantum Dot Fluorophores. *J. Am. Chem. Soc.* **2005**, *127*, 3870–3878.
5. Dorokhin, D.; Tomczak, N.; Han, M. Y.; Reinhoudt, D. N.; Velders, A. H.; Vancso, G. J. Reversible Phase Transfer of (CdSe/ZnS) Quantum Dots between Organic and Aqueous Solutions. *ACS Nano* **2009**, *3*, 661–667.
6. Medintz, I. L.; Uyeda, H. T.; Goldman, E. R.; Mattoussi, H. Quantum Dot Bioconjugates for Imaging, Labelling and Sensing. *Nat. Mater.* **2005**, *4*, 435–446.
7. Sperling, R. A.; Liedl, T.; Duhr, S.; Kudera, S.; Zanella, M.; Lin, J.; Chang, W. H.; Braun, D.; Parak, W. J. Size Determination of (Bio)conjugated Water-Soluble Colloidal Nanoparticles: A Comparison of Different Techniques. *J. Phys. Chem. C* **2007**, *111*, 11552–11559.
8. Zhang, Y.; Clapp, A. Overview of Stabilizing Ligands for Biocompatible Quantum Dot Nanocrystals. *Sensors* **2011**, *11*, 11036–11055.
9. Baker, M. Nanotechnology Imaging Probes: Smaller and More Stable. *Nat. Methods* **2010**, *7*, 957–962.
10. Pinaud, F.; Clarke, S.; Sittner, A.; Dahan, M. Probing Cellular Events, One Quantum Dot at a Time. *Nat. Methods* **2010**, *7*, 275–285.
11. Gerion, D.; Pinaud, F.; Williams, S. C.; Parak, W. J.; Zanchet, D.; Weiss, S.; Alivisatos, A. P. Synthesis and Properties of Biocompatible Water-Soluble Silica-Coated CdSe/ZnS Semiconductor Quantum Dots. *J. Phys. Chem. B* **2001**, *105*, 8861–8871.
12. Yoffe, A. D. Semiconductor Quantum Dots and Related Systems: Electronic, Optical, Luminescence and Related Properties of Low Dimensional Systems. *Adv. Phys.* **2001**, *50*, 1–208.
13. Groc, L.; Lafourcade, M.; Heine, M.; Renner, M.; Racine, V.; Sibarita, J.-B.; Lounis, B.; Choquet, D.; Cognet, L. Surface Trafficking of Neurotransmitter Receptor: Comparison between Single-Molecule/Quantum Dot Strategies. *J. Neurosci.* **2007**, *27*, 12433–12437.
14. Howarth, M.; Liu, W.; Puthenveetil, S.; Zheng, Y.; Marshall, L. F.; Schmidt, M. M.; Wittrup, K. D.; Bawendi, M. G.; Ting, A. Y. Monovalent, Reduced-Size Quantum Dots for Imaging Receptors on Living Cells. *Nat. Methods* **2008**, *5*, 397–399.
15. Kim, Y.; Kim, S. H.; Tanyeri, M.; Katzenellenbogen, J. A.; Schroeder, C. M. Dendrimer Probes for Enhanced Photostability and Localization in Fluorescence Imaging. *Biophys. J.* **2013**, *104*, 1566–1575.
16. Choi, H. S.; Liu, W.; Misra, P.; Tanaka, E.; Zimmer, J. P.; Ipe, B. I.; Bawendi, M. G.; Frangioni, J. V. Renal Clearance of Quantum Dots. *Nat. Biotechnol.* **2007**, *25*, 1165–1170.
17. Maeda, H.; Wu, J.; Sawa, T.; Matsumura, Y.; Hori, K. Tumor Vascular Permeability and the EPR Effect in Macromolecular Therapeutics: A Review. *J. Controlled Release* **2000**, *65*, 271–284.
18. Jain, R. K.; Stylianopoulos, T. Delivering Nanomedicine to Solid Tumors. *Nat. Rev. Clin. Oncol.* **2010**, *7*, 653–664.
19. Cheng, Y.; Meyers, J. D.; Broome, A. M.; Kenney, M. E.; Basilion, J. P.; Burda, C. Deep Penetration of a PDT Drug into Tumors by Noncovalent Drug-Gold Nanoparticle Conjugates. *J. Am. Chem. Soc.* **2011**, *133*, 2583–2591.
20. Wu, X.; He, X.; Wang, K.; Xie, C.; Zhou, B.; Qing, Z. Ultrasmall Near-Infrared Gold Nanoclusters for Tumor Fluorescence Imaging *in Vivo*. *Nanoscale* **2010**, *2*, 2244–2249.
21. Oh, E.; Delehanty, J. B.; Sapsford, K. E.; Susumu, K.; Goswami, R.; Blance-Canosa, J. B.; Dawson, P. E.; Granek, J.; Shoff, M.; Zhang, Q.; Goering, P. L.; Huston, A.; Medintz, I. L. Cellular Uptake and Fate of PEGylated Gold Nanoparticle Is Dependent on Both Cell-Penetration Peptides and Particle Size. *ACS Nano* **2011**, *5*, 6434–6448.
22. Faucher, L.; Tremblay, M.; Lagueux, J.; Gossuin, Y.; Fortin, M.-A. Rapid Synthesis of PEGylated Ultrasmall Gadolinium Oxide Nanoparticles for Cell Labeling and Tracking with MRI. *ACS Appl. Mater. Interfaces* **2012**, *4*, 4506–4515.
23. Zeng, L.; Ren, W.; Zheng, L.; Cui, P.; Wu, A. Ultrasmall Water-Soluble Metal-Iron Oxide Nanoparticles as T_1-Weighted Contrast Agents for Magnetic Resonance Imaging. *Phys. Chem. Chem. Phys.* **2012**, *14*, 2631–2636.
24. Sun, Y.-P.; Zhou, B.; Lin, Y.; Wang, W.; Fernando, K. A. S.; Pathak, P.; Meziani, M. J.; Harruff, B. A.; Wang, X.; Wang, H.; *et al*. Quantum-Sized Carbon Dots for Bright and Colorful Photoluminescence. *J. Am. Chem. Soc.* **2006**, *128*, 7756–7757.
25. Cao, L.; Wang, X.; Meziani, M. J.; Lu, F.; Wang, H.; Luo, P. G.; Lin, Y.; Harruff, B. A.; Veca, L. M.; Murray, D.; *et al*. Carbon Dots for Multiphoton Bioimaging. *J. Am. Chem. Soc.* **2007**, *129*, 11318–11319.
26. Bourlinos, A. B.; Stassinopoulos, A.; Anglos, D.; Zboril, R.; Karakassides, M.; Giannelis, E. P. Surface Functionalized Carbogenic Quantum Dots. *Small* **2008**, *4*, 455–458.
27. Bourlinos, A. B.; Stassinopoulos, A.; Anglos, D.; Zboril, R.; Georgakilas, V.; Giannelis, E. P. Photoluminescent Carbogenic Dots. *Chem. Mater.* **2008**, *20*, 4539–4541.
28. Peng, H.; Travas-Sejdic, J. Simple Aqueous Solution Route to Luminescent Carbogenic Dots from Carbohydrates. *Chem. Mater.* **2009**, *21*, 5563–5565.
29. Mochalin, V. N.; Gogotsi, Y. Wet Chemistry Route to Hydrophobic Blue Fluorescent Nanodiamond. *J. Am. Chem. Soc.* **2009**, *131*, 4594–4595.
30. Yang, S.-T.; Cao, L.; Luo, P. G.; Lu, F.; Wang, X.; Wang, H.; Meziani, M. J.; Liu, Y.; Qi, G.; Sun, Y.-P. Carbon Dots for Optical Imaging *in Vivo*. *J. Am. Chem. Soc.* **2009**, *131*, 11308–11309.
31. Yang, S.-T.; Wang, X.; Wang, H.; Lu, F.; Luo, P. G.; Cao, L.; Meziani, M. J.; Liu, J.-H.; Liu, Y.; Chen, M.; *et al*. Carbon Dots as Nontoxic and High-Performance Fluorescence Imaging Agents. *J. Phys. Chem. C* **2009**, *113*, 18110–18114.
32. Li, Q.; Ohulchanskyy, T. Y.; Liu, R.; Koynov, K.; Wu, D.; Best, A.; Kumar, R.; Bonoiu, A.; Prasad, P. N. Photoluminescent Carbon Dots as Biocompatible Nanoprobes for Targeting Cancer Cells *in Vitro*. *J. Phys. Chem. C* **2010**, *114*, 12062–12068.
33. Li, H.; He, X.; Kang, Z.; Huang, H.; Liu, Y.; Liu, J.; Lian, S.; Tsang, C. H. A.; Yang, X.; Lee, S.-T. Water-Soluble Fluorescent Carbon Quantum Dots and Photocatalyst Design. *Angew. Chem., Int. Ed.* **2010**, *49*, 4430–4434.
34. Wang, X.; Cao, L.; Yang, S.-T.; Lu, F.; Meziani, M. J.; Tian, L.; Sun, K. W.; Bloodgood, M. A.; Sun, Y.-P. Bandgap-Like Strong Fluorescence in Functionalized Carbon Nanoparticles. *Angew. Chem., Int. Ed.* **2010**, *49*, 5310–5314.
35. Chandra, S.; Das, P.; Bag, S.; Laha, D.; Pramanik, P. Synthesis, Functionalization and Bioimaging Applications of Highly Fluorescent Carbon Nanoparticles. *Nanoscale* **2011**, *3*, 1533–1540.
36. Bourlinos, A. B.; Zboril, R.; Petr, J.; Bakandritsos, A.; Krysmann, M.; Giannelis, E. P. Luminescent Surface Quaternized Carbon Dots. *Chem. Mater.* **2012**, *24*, 6–8.
37. Tao, H.; Yang, K.; Ma, Z.; Wan, J.; Zhang, Y.; Kang, Z.; Liu, Z. *In Vivo* NIR Fluorescence Imaging, Biodistribution, and Toxicology of Photoluminescent Carbon Dots Produced

from Carbon Nanotubes and Graphite. *Small* **2012**, *8*, 281–290.
38. Li, H.; Kang, Z.; Liu, Y.; Lee, S.-T. Carbon Nanodots: Synthesis, Properties and Applications. *J. Mater. Chem.* **2012**, *22*, 24230–24253.
39. Luo, P. G.; Sahu, S.; Yang, S.-T.; Sonkar, S. K.; Wang, J.; Wang, H.; LeCroy, G. E.; Cao, L.; Sun, Y.-P. Carbon "Quantum" Dots for Optical Bioimaging. *J. Mater. Chem. B* **2013**, *1*, 2116–2127.
40. Cao, L.; Meziani, M. J.; Sahu, S.; Sun, Y.-P. Photoluminescence Properties of Graphene *versus* Other Carbon Nanomaterials. *Acc. Chem. Res.* **2013**, *46*, 171–180.
41. Liu, Z.; Zu, Y.; Fu, Y.; Zhang, Z.; Meng, R. Assembling and Imaging of His-Tag Green Fluorescent Protein on Mica Surfaces Studied by Atomic Force Microscopy and Fluoresence Microscopy. *Microsc. Res. Technol.* **2008**, *71*, 802–809.
42. Yang, F.; Moss, L. G.; Phillips, G. N. The Molecular Structure of Green Fluorescent Proteins. *Nat. Biotechnol.* **1996**, *14*, 1246–1251.
43. Prachayasittikul, V.; Isarankura-Na-Ayudhya, C.; Hilterhaus, L.; Hinz, A.; Tantimongcolwat, T.; Galla, H. Interaction Analysis of Chimeric Metal-Binding Green Fluorescent Protein and Artificial Solid-Supported Lipid Membrane by Quartz Crystal Microbalance and Atomic Force Microscopy. *J. Biochem. Biophys. Res. Commun.* **2005**, *327*, 174–182.
44. Andrews, P. Estimation of the Molecular Weights of Proteins by Sephadex Gel-Filtration. *Biochem. J.* **1964**, *91*, 222–233.
45. Xu, J.; Sahu, S.; Cao, L.; Anilkumar, P.; Tackett, K. N., II; Qian, H.; Bunker, C. E.; Guliants, E. A.; Parenzan, A.; Sun, Y.-P. Carbon Nanoparticles as Chromophores for Photon Harvesting and Photoconversion. *ChemPhysChem* **2011**, *12*, 3604–3608.
46. Xu, J.; Sahu, S.; Cao, L.; Bunker, C. E.; Peng, G.; Liu, Y.; Fernando, K. A. S.; Wang, P.; Guliants, E. A.; Meziani, M. J.; *et al.* Efficient Fluorescence Quenching in Carbon Dots by Surface-Doped Metals - Disruption of Excited State Redox Processes and Mechanistic Implications. *Langmuir* **2012**, *28*, 16141–16147.
47. Bunker, C. E.; Sun, Y.-P. Evidence for Enhanced Bimolecular Reactions in Supercritical CO_2 at Near-Critical Densities from a Time-Resolved Study of Fluorescence Quenching of 9,10-Bis(phenylethynyl)anthracene by Carbon Tetrabromide. *J. Am. Chem. Soc.* **1995**, *117*, 10865–10870.
48. Lakowicz, J. R. *Principles of Fluorescence Spectroscopy*; Springer: NJ, 2006.
49. Patterson, G.; Day, R. N.; Piston, D. Fluorescent Protein Spectra. *J. Cell Sci.* **2001**, *114*, 837–838.
50. Spectral Database for Organic Compounds. National Institute of Advanced Industrial Science and Technology (AIST), Japan (http://sdbs.db.aist.go.jp/sdbs/cgi-bin/cre_index.cgi).
51. Sadtler Infrared Spectral Database, Bio-Rad, USA (http://www.bio-rad.com/en-us/category/ir).
52. Day, N. R.; Davidson, M. W. The Fluorescent Protein Palette: Tools for Cellular Imaging. *Chem. Soc. Rev.* **2009**, *38*, 2887–2921.